Localization of Delaminations in Composite Laminates by Nonlinear Interface Stresses

WEI XU, MACIEJ RADZIENSKI, MAOSEN CAO
and WIESLAW OSTACHOWITZ

ABSTRACT

While often barely visible, delaminations in composite laminates can critically degrade structural performance and safety. However, localizing small delaminations that minimally alter local stiffnesses remains challenging. On the other hand, contact-induced nonlinearity arises when a delamination periodically closes and opens like breathing, resulting in time-varying normal and shear stresses across the delamination interfaces. This study defines these stresses as nonlinear interface stresses (NISs), emphasizing their application to the localization of delaminations in composite laminates. The NISs exclusively appear within "breathing" delaminations, acting as multi-tone harmonic excitation sources that produce higher harmonics. Additionally, the NISs can serve as ideal indicators for localizing delaminations due to their inherently localized nature. The NISs are reconstructed from nonlinear steady-state wavefields (NSWs) of composite laminates at higher harmonics. The approach based on NISs is experimentally validated on a glass fiber-reinforced polymer laminated plate containing multiple local delaminations fabricated using Teflon sheets, low-speed impacts, and local heating. A piezoelectric actuator, mounted at the center of the plate, generates single-tone harmonic excitations, while a scanning laser Doppler vibrometer measures the NSW of the plate. The experimental results reveal that not only large thermal delaminations but also small delaminations caused by Teflon inserts and low-speed impacts can be spatially characterized with locations and sizes.

INTRODUCTION

Composite laminates are widely used in engineering structures because of their high strength and stiffness. However, they are prone to local delaminations. Localizing small delaminations in composite laminates is challenging because their local stiffnesses are minimally altered.

Wei Xu, Institute of Fluid-Flow Machinery, Polish Academy of Sciences, 14 Fiszera Street, Gdańsk 80-231, Poland
Maciej Radzieński, Institute of Fluid-Flow Machinery, Polish Academy of Sciences, 14 Fiszera Street, Gdańsk 80-231, Poland
Maosen Cao, Hohai University, 1 Xikang Road, Nanjing 210098, China
Wiesław Ostachowicz (corresponding author), Institute of Fluid-Flow Machinery, Polish Academy of Sciences, 14 Fiszera Street, Gdańsk 80-231, Poland

Recent advances in delamination localization have increasingly focused on nonlinear characteristics, such as nonlinear harmonics, by exploiting the dynamic behaviour of delamination at contact interfaces. Traditionally, two primary models describe delamination behaviour. The first model is governed by the "constrained mode", where debonded layers separate while maintaining identical transverse displacements; the second model is governed by the "free mode", which permits separation but does not prevent interpenetration [1]. A more advanced model governed by the "breathing mode" allows debonded layers to cyclically contact and separate, producing a characteristic opening-closing motion [2]. The nonlinear harmonics generated by this "breathing" behaviour have emerged as effective delamination indicators [3]. This led to the concept of contact acoustic nonlinearity (CAN), a form of nonlinearity arising from stress interactions at contact interfaces, particularly in "clapping" and "rubbing" patterns [4]. Building on this concept, nonlinear elastic wave spectroscopy (NEWS) was developed to analyze nonlinear harmonics for damage assessment [5, 6]. Solodov [4] pioneered the use of ultrasonic waves to probe interfacial CAN, establishing multiple nonlinear non-destructive testing (NDT) techniques. These methods excel at detecting subtle fractures that linear NDT approaches often miss. Leveraging nonlinear harmonics in vibro-acoustic response spectra, NEWS-based techniques have been widely adopted for delamination detection [5–8]. Recent studies further demonstrate the effectiveness of nonlinear harmonics in diverse delamination scenarios [9–13].

Time-varying normal and shear stresses at delamination interfaces are known to generate nonlinear harmonics [2]. While these harmonics effectively indicate the presence and extent of delaminations, they cannot directly characterize their locations and sizes. Recent advances have introduced nonlinear interface forces (NIFs) in laminated beams, which arise exclusively in "breathing" delamination regions. These NIFs act as multi-tone harmonic excitation sources, producing higher harmonics [14]. By taking advantage of this behaviour, NIFs can be reconstructed from nonlinear operating deflection shapes to localize debonding. Building on the NIF framework, this study formulates nonlinear interface stresses (NISs) across "breathing" delaminations, with a focus on their application for precise delamination localization in composite laminates.

NONLINEAR INTERFACE STRESSES FOR DELAMINATION LOCALIZATION

A cross-ply composite laminate, composed of N layers with 0/90º orientations, is subjected to a transverse harmonic excitation at an angular frequency ω_e. A delamination occurs between the nth and (n+1)th layers of the composite laminate, dividing the structure into two distinct sections: Section I comprising the 1st to nth layers and Section II comprising the (n+1)th to Nth layers. The equation of out-of-plane motion for Section I can be expressed as

$$D_{11}\frac{\partial^4 w}{\partial x^4}+2(D_{12}+2D_{66})\frac{\partial^4 w}{\partial x^2\partial y^2}+D_{22}\frac{\partial^4 w}{\partial y^4}+\overline{\rho}\frac{\partial^2 w}{\partial t^2}=\sigma_z-\frac{h}{2}\left(\frac{\partial \tau_{zx}}{\partial x}+\frac{\partial \tau_{zy}}{\partial y}\right), \quad (1)$$

where D_{ij} denote stiffness coefficients of Section I, $w(x,y,t)$ denotes its out-of-plane displacement, h denotes its thickness, $\overline{\rho}$ denotes its average density across the midsurface. Normal stress σ_z and shear stresses τ_{zx} and τ_{zy} are distributed

across the interfaces between Sections I and II. Note that the wavelength across the composite laminate should be much larger than its thickness to ensure the validity of Eq. (1), as it is established based on Kirchhoff plate theory. Under the single-tone harmonic excitation, the "breathing" delamination periodically opens and closes. Based on the NIF model for a laminated beam [14], the normal and shear stresses across the interfaces are assumed to appear exclusively within the delamination region labelled as Ω (as illustrated in Fig. 1) and comprise multi-tone components:

$$\sigma_z(x,y,t)=\begin{cases}\sigma_{z1}(x,y,t) & x,y\notin\Omega\\ \sum_{m=1}^{M}\sigma_{zm}(x,y,t) & x,y\in\Omega\end{cases}, \tag{2.1}$$

$$\tau_{zx}(x,y,t)=\begin{cases}\tau_{zx1}(x,y,t) & x,y\notin\Omega\\ \sum_{m=1}^{M}\tau_{zxm}(x,y,t) & x,y\in\Omega\end{cases}, \tag{2.2}$$

$$\tau_{zy}(x,y,t)=\begin{cases}\tau_{zy1}(x,y,t) & x,y\notin\Omega\\ \sum_{m=1}^{M}\tau_{zym}(x,y,t) & x,y\in\Omega\end{cases}, \tag{2.3}$$

When the delamination fully opens, the "free mode" applies and the delamination interface belonging to Section I becomes a free surface, leading to the vanishment of normal and shear stresses. When the delamination is completely closed, the "constrained mode" applies, resulting in maximum normal and shear stresses that approximate those across the bonded interfaces. A cosine-form function is used to represent the periodic and continuous variation of the NISs during the opening-closing motion of the "breathing" delamination:

$$\sigma_{zm}(x,y,t)=\frac{1}{2}\Sigma_{zm}(x,y)(1+\cos\omega_{\mathrm{B}}t)\cos(\omega_m t+\phi_{zm}), \tag{3.1}$$

$$\tau_{zxm}(x,y,t)=\frac{1}{2}\mathrm{T}_{zxm}(x,y)(1+\cos\omega_{\mathrm{B}}t)\cos(\omega_m t+\phi_{zxm}), \tag{3.2}$$

$$\tau_{zym}(x,y,t)=\frac{1}{2}\mathrm{T}_{zym}(x,y)(1+\cos\omega_{\mathrm{B}}t)\cos(\omega_m t+\phi_{zym}), \tag{3.3}$$

in which the "breathing" frequency ω_{B} satisfies $\omega_{\mathrm{B}}=\omega_{\mathrm{e}}$, and amplitudes Σ_{zm}, T_{zxm}, and T_{zym} as well as phases ϕ_{zm}, ϕ_{zxm}, and ϕ_{zym} are associated with σ_{zm}, τ_{zxm}, and τ_{zym} for the totally closed status, respectively. As outlined in Eq. (3), the opening-closing motion of the "breathing" delamination modulates the NISs, leading to the multi-tone components of NIFs within the delamination:

$$\sigma_z(x,y,t)=\sum_{m=1}^{M}\Sigma_{zm}(x,y)\cos(\omega_m t+\phi_{zm}), \tag{4.1}$$

$$\tau_{zx}(x,y,t)=\sum_{m=1}^{M}\mathrm{T}_{zxm}(x,y)\cos(\omega_m t+\phi_{zxm}), \tag{4.2}$$

$$\tau_{zy}(x,y,t)=\sum_{m=1}^{M}\mathrm{T}_{zym}(x,y)\cos(\omega_m t+\phi_{zym}). \tag{4.3}$$

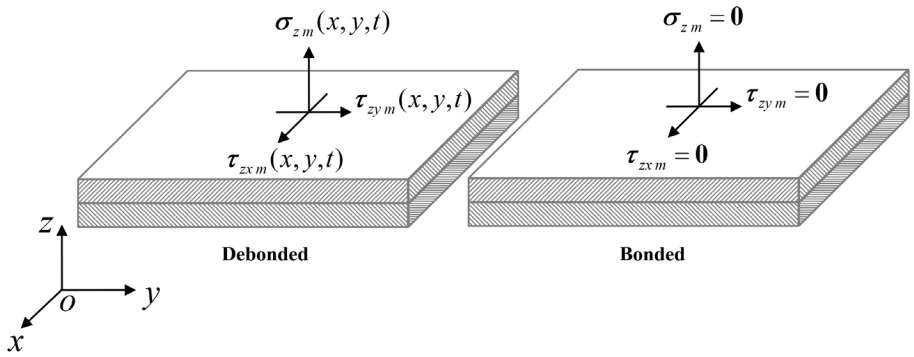

Figure 1. NISs across the interfaces of debonded and bonded elements of a composite laminate

Extending a proof from 1D to 2D [14], ω_m can be expressed as successive multiples of ω_{e}

$$\omega_m = m\omega_{\mathrm{e}}. \tag{5}$$

As specified in Eq. (4), NIFs consist of multiple components associated with higher harmonics at $m\omega_{\mathrm{e}}$ (m=1, 2, 3, . . .). Physically, the NISs are exclusively applied to the "breathing" delamination as multi-tone harmonic excitation sources to produce nonlinear harmonics. The waveform at each measurement point of the composite laminate can be expressed as a superposition of higher harmonics:

$$w(x,y,t)=\sum_{m=1}^{M} w_m(x,y,t)=\sum_{m=1}^{M} W_m(x,y)\cos(\omega_m t+\phi_m), \tag{6}$$

where $W_m(x,y)$ and ϕ_m denote the amplitude and phase of the mth component $w_m(x,y,t)$ of the waveform, respectively. Substituting Eqs. (4) and (6) into Eq. (1) yields

$$D_{11}^{\mathrm{I}}\frac{\partial^4 W_m}{\partial x^4}+2(D_{12}^{\mathrm{I}}+2D_{66}^{\mathrm{I}})\frac{\partial^4 W_m}{\partial x^2\partial y^2}+D_{22}^{\mathrm{I}}\frac{\partial^4 W_m}{\partial y^4}-\omega_m^2\overline{\rho}^{\mathrm{I}}W_m=\Sigma_{z\,m}-\frac{h}{2}\left(\frac{\partial \mathrm{T}_{zx\,m}}{\partial x}+\frac{\partial \mathrm{T}_{zy\,m}}{\partial y}\right), \tag{7}$$

where $W_m(x,y)$ from all measurement points constitute the mth component of the wavefield. It is noteworthy that the first component of the SW is referred to as the linear SW (LSW), while higher-order components of the SW are classified as the nonlinear SWs (NSWs). A DI $DI_m(x,y)$ is derived from Eq. (7), which appears exclusively in the delamination region and can be used to spatially characterize delamination locations and sizes:

$$\begin{aligned} DI_m(x,y) &= \left|\Sigma_{z\,m}-\frac{h}{2}\left(\frac{\partial \mathrm{T}_{zx\,m}}{\partial x}+\frac{\partial \mathrm{T}_{zy\,m}}{\partial y}\right)\right| \\ &= \left|D_{11}^{\mathrm{I}}\frac{\partial^4 W_m}{\partial x^4}+2(D_{12}^{\mathrm{I}}+2D_{66}^{\mathrm{I}})\frac{\partial^4 W_m}{\partial x^2\partial y^2}+D_{22}^{\mathrm{I}}\frac{\partial^4 W_m}{\partial y^4}-\omega_m^2\overline{\rho}^{\mathrm{I}}W_m\right|. \end{aligned} \tag{8}$$

DELAMINATION LOCALIZATION IN A COMPOSITE LAMINATE

The experimental specimen consists of a 500 mm × 500 mm × 2 mm glass fiber-reinforced polymer (GFRP) laminated plate with 12 layers (see Fig. 2 for the front surface view), containing eleven artificially fabricated delaminations classified into three types (outlined in Table 1): Teflon-inserts-caused (type-I), impact-caused (type-

II), and local-heating-caused (type-III) delaminations. A schematic of the delaminations in the GFRP laminated plate is shown in Fig. 3. Four type-I delaminations, labelled D1, D2, D3, and D4, were fabricated by inserting four green circular Teflon inserts, each with a diameter of 10 millimetres. Counting from the front surface, the delaminations D1, D2, D3, and D4 are located between the 2nd and 3rd layers, 4th and 5th layers, 8th and 9th layers, and 6th and 7th layers, respectively. Four type-II delaminations, labelled D5, D6, D7, and D8, were created by dropping weights onto the front surface of the plate with energies of 5 J, 10 J, 15 J, and 2.5 J, respectively. Three type-III delaminations, labelled D9, D10, and D11, were induced by locally heating the front surface of the plate to a temperature of around 500°C, resulting in thermal delaminations with approximate diameters of 30, 20, and 27 millimetres, respectively. It is noteworthy that delaminations D10 and D11 spatially cover delaminations D4 and D8, respectively; therefore, delaminations D4 and D8 will not be referred to hereinafter to avoid confusion with D10 and D11. A piezoelectric patch mounted at the plate's center provides single-tone harmonic excitation, and a scanning laser Doppler vibrometer (SLDV) measures structural waves across a 333 × 333 grid of measurement points, with dimensionless coordinates $\zeta = x/500$ and $\eta = y/500$ respectively.

Table 1 Locations and dimensions of the delaminations in the GFRP laminated plate.

Type	Label	x [mm]	y [mm]	Diameter [mm]	Dimensionless coordinates
Teflon	D1	250	375	10	$\zeta\in[0.49,0.51]$ $\eta\in[0.74,0.76]$
	D2	125	250	10	$\zeta\in[0.24,0.26]$ $\eta\in[0.49,0.51]$
	D3	250	125	10	$\zeta\in[0.49,0.51]$ $\eta\in[0.24,0.26]$
	D4	375	250	10	$\zeta\in[0.74,0.76]$ $\eta\in[0.49,0.51]$
Impact	D5	125	375	9.6	$\zeta\in[0.240,0.260]$ $\eta\in[0.740,0.760]$
	D6	125	125	12.8	$\zeta\in[0.237,0.263]$ $\eta\in[0.237,0.263]$
	D7	375	125	14.5	$\zeta\in[0.736,0.764]$ $\eta\in[0.236,0.264]$
	D8	375	375	7.8	$\zeta\in[0.742,0.758]$ $\eta\in[0.742,0.758]$
Heating	D9	113	187	30	$\zeta\in[0.196,0.256]$ $\eta\in[0.344,0.404]$
	D10	375	250	20	$\zeta\in[0.73,0.77]$ $\eta\in[0.48,0.52]$
	D11	375	375	27	$\zeta\in[0.723,0.777]$ $\eta\in[0.723,0.777]$

Figure 2. Experimental specimen: the GFRP laminated plate with multiple delaminations

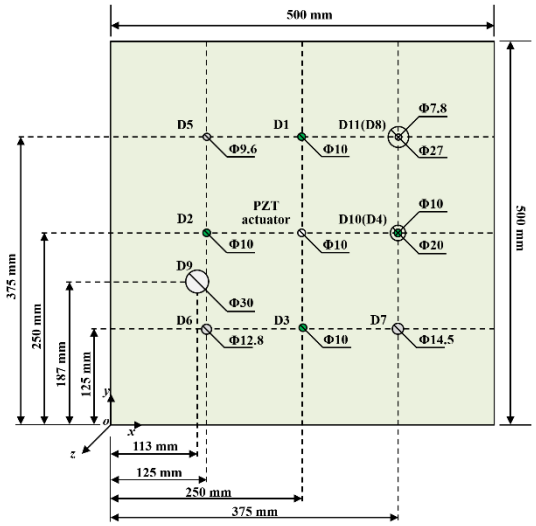

Figure 3. Schematic of the delaminations in the GFRP laminated plate

The GFRP laminated plate is excited at one of its natural frequencies of 16528 Hz, with a 256 kHz sampling frequency. The steady-state velocity response near the plate's center reveals that the 1st harmonic distinctly appears at the excitation frequency ω_e, whereas the second and third harmonics appear at its double and triple frequencies, respectively, but are significantly weaker in comparison. In contrast to the 2nd harmonic, the 3rd harmonic is more observable. Consequently, the NSW associated with the 3rd harmonic (Fig. 4) is selected for analysis. The DI is calculated by Eq. (8), as shown in Fig. 5(a), with its maximum being unity. The peaks in the DI successfully image all three thermal delaminations (D9-D11), two Teflon-insert delaminations (D2-D3), and two impact-induced delaminations (D6-D7), precisely matching their actual locations (Table 1, Fig. 3). Notably, DI values near the central PZT actuator were nullified to eliminate excitation effects. Nevertheless, two delaminations remained undetected: D1 (deepest from measurement surface) and D5 (lowest impact energy), as their minimal breathing motions generate insufficient nonlinearity for detection.

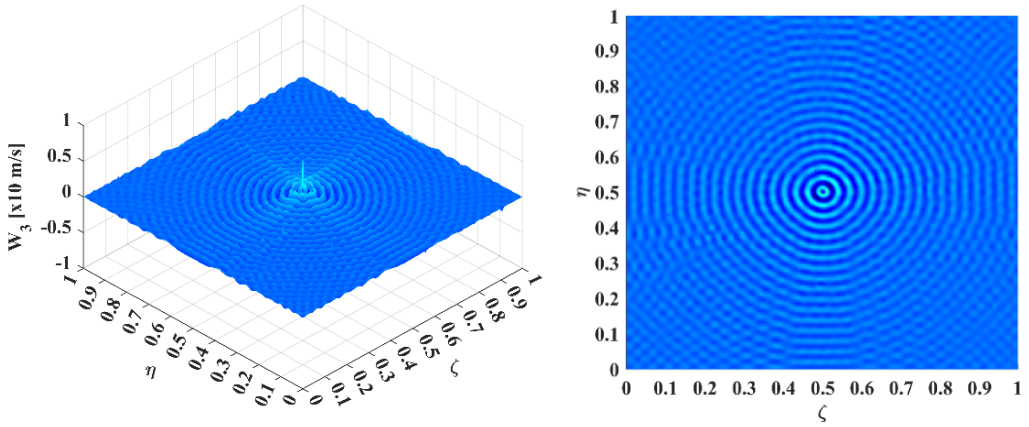

(a) (b)

Figure 4. (a) NSW associated with the 3rd harmonics and (b) its planform.

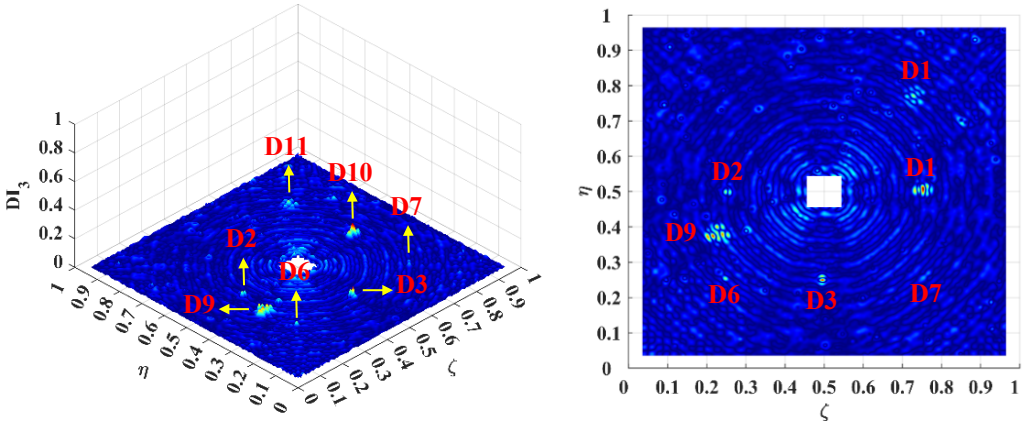

(a) (b)

Figure 5. (a) DI for the NSW associated with the 3rd harmonic and (b) its planform.

CONCLUSIONS

This study introduces the NISs across "breathing" delaminations, with emphasis on their application to the localization of delaminations in composite laminates. The NISs exclusively appear in "breathing" delaminations, acting as multi-tone harmonic excitation sources that produce higher harmonics. Their inherently localized nature makes them ideal indicators for precise delamination imaging. The approach's capability is experimentally validated on a GFRP laminated plate with multiple local delaminations fabricated by Teflon inserts, low-speed impacts, and local heating. The results demonstrate the method's effectiveness in detecting both large thermal delaminations and smaller defects caused by Teflon inserts or low-energy impacts. This capability provides a powerful tool for graphically characterizing early-stage delamination configurations in composite structures.

ACKNOWLEDGMENTS

Wei Xu is grateful to the support of the China-CEEC Joint Education Project, Grant No. 2023288, and the CSC Scholarship, Grant No. 202306710027.

REFERENCES

1. Mujumdar, P. and Suryanarayan, S. 1988. "Flexural vibration of beams with delaminations", Journal of *Sound and Vibration*, 125(3): 441-461.
2. Bovsunovsky, A. and Surace, C. 2015. "Non-linearities in the vibrations of elastic structures with a closing crack: A state of the art review", *Mechanical Systems and Signal Processing*, 62-63: 129-148
3. Zarembo, L., Krasilnikov, V., Sluch, V., and Serdobolskaya, O. 1966. "On some phenomena accompanying forced non-linear vibrations of acoustic resonators", *Akust. Zh.*, 12: 486-487.
4. Solodov, I. 1998. "Ultrasonics of non-linear contacts: propagation, reflection and NDE-applications", *Ultrasonics*, 36(1-5): 383-390.
5. Van Den Abeele, K., Johnson, P., and Sutin, A. 2000. "Nonlinear elastic wave spectroscopy (NEWS) techniques to discern material damage, Part I: *Research in Nondestructive Evaluation*, 12(1): 17-30.
6. Van Den Abeele, K., Carmeliet, J., Ten Cate, J.A., and Johnson, P. 2000. "Nonlinear elastic wave spectroscopy (NEWS) techniques to discern material damage, Part II: *Research in Nondestructive Evaluation*, 12(1): 31-42.
7. Meo, M. and Zumpano, G. 2005. "Nonlinear elastic wave spectroscopy identification of impact damage on a sandwich plate", *Composite Structures*, 71(3-4): 469-474.
8. Meo, M., Polimeno, U., and Zumpano, G. 2008. "Detecting damage in composite material using nonlinear elastic wave spectroscopy methods", *Applied Composite Materials*, 15(3): 115-126.
9. Czelusniak, K., Staszewski, W.J., and Aymerich, F. 2022. "Local bispectral characteristics of nonlinear vibro-acoustic modulations for structural damage detection", *Mechanical Systems and Signal Processing*, 178: 109199.
10. He, Y., Xiao, Y., Su, Z., Pan, Y., and Zhang, Z. 2022. "Contact acoustic nonlinearity effect on the vibro-acoustic modulation of delaminated composite structures", *Mechanical Systems and Signal Processing*, 163: 108161.
11. Ehsani, M., Shamshirsaz, M., Sadighi, M., Sepehry, N., and Loendersloot, R. 2023. "Theoretical and experimental investigations on control parameters of piezo-based vibro-acoustic modulation health monitoring of contact acoustic nonlinearity in a sandwich beam", *Applied Acoustics*, 203: 109193.
12. Willmann, E., Boll, B., Scheel, M., Meissner, R.H., and Fiedler, B. 2023. "Health monitoring of CFRP laminates under cyclic loading via vibro-acoustic modulation based measurements", *Composite Structures*, 308: 116696.
13. Willmann, E., Boll, B., Mikaelyan, G., Wittich, H., Meissner, R.H., and Fiedler, B. 2023. "Vibro-acoustic modulation based measurements in CFRP laminates for damage detection in Open-Hole structures", *Composites Communications*, 42: 101659.
14. Xu, W., Wu, X., Ji, M., Yang, Y., Cao, M., Radzieński, M., and Ostachowicz, W. 2025. "Nonlinear interface forces in "breathing" debondings of laminated beams: From formation mechanism to debonding localization", *Journal of Sound and Vibration*, 603: 118979.